Cell Metabolism
Article

Partial and Transient Reduction of Glycolysis by PFKFB3 Blockade Reduces Pathological Angiogenesis

Sandra Schoors,[1,2,8] Katrien De Bock,[1,2,8] Anna Rita Cantelmo,[1,2,8] Maria Georgiadou,[1,2,8] Bart Ghesquière,[1,2] Sandra Cauwenberghs,[1,2] Anna Kuchnio,[1,2] Brian W. Wong,[1,2] Annelies Quaegebeur,[1,2] Jermaine Goveia,[1,2] Francesco Bifari,[1,2] Xingwu Wang,[1,2] Raquel Blanco,[3] Bieke Tembuyser,[1,2] Ivo Cornelissen,[1,2] Ann Bouché,[1,2] Stefan Vinckier,[1,2] Santiago Diaz-Moralli,[4] Holger Gerhardt,[3,5,6] Sucheta Telang,[7] Marta Cascante,[4] Jason Chesney,[7] Mieke Dewerchin,[1,2,9] and Peter Carmeliet[1,2,9,*]

[1]Laboratory of Angiogenesis and Neurovascular link, Vesalius Research Center, Department of Oncology, University of Leuven, Leuven 3000, Belgium
[2]Laboratory of Angiogenesis and Neurovascular link, Vesalius Research Center, VIB, Leuven 3000, Belgium
[3]Vascular Biology Laboratory, London Research Institute, Cancer Research UK, London WC2A 3LY, UK
[4]Department of Biochemistry and Molecular Biology and IBUB, Universitat de Barcelona, Barcelona 08007, Spain
[5]Vascular Patterning Laboratory, Vesalius Research Center, University of Leuven, Leuven 3000, Belgium
[6]Vascular Patterning Laboratory, Vesalius Research Center, VIB, Leuven 3000, Belgium
[7]James Graham Brown Cancer Center, University of Louisville, Louisville, KY 40202, USA
[8]These authors contributed equally to this work and are co-first authors
[9]These authors contributed equally to this work and are co-last authors
*Correspondence: peter.carmeliet@vib-kuleuven.be
http://dx.doi.org/10.1016/j.cmet.2013.11.008

SUMMARY

Strategies targeting pathological angiogenesis have focused primarily on blocking vascular endothelial growth factor (VEGF), but resistance and insufficient efficacy limit their success, mandating alternative antiangiogenic strategies. We recently provided genetic evidence that the glycolytic activator phosphofructokinase-2/fructose-2,6-bisphosphatase 3 (PFKFB3) promotes vessel formation but did not explore the antiangiogenic therapeutic potential of PFKFB3 blockade. Here, we show that blockade of PFKFB3 by the small molecule 3-(3-pyridinyl)-1-(4-pyridinyl)-2-propen-1-one (3PO) reduced vessel sprouting in endothelial cell (EC) spheroids, zebrafish embryos, and the postnatal mouse retina by inhibiting EC proliferation and migration. 3PO also suppressed vascular hyperbranching induced by inhibition of Notch or VEGF receptor 1 (VEGFR1) and amplified the antiangiogenic effect of VEGF blockade. Although 3PO reduced glycolysis only partially and transiently in vivo, this sufficed to decrease pathological neovascularization in ocular and inflammatory models. These insights may offer therapeutic antiangiogenic opportunities.

INTRODUCTION

Angiogenesis stimulates the progression of numerous disorders. Hence, targeting this process by blocking angiogenic signals such as vascular endothelial growth factor (VEGF) has become a clinically attractive strategy (Singh and Ferrara, 2012). However, insufficient efficacy and resistance limit its success (Ebos and Kerbel, 2011; Potente et al., 2011). Although combination treatment with multiple agents blocking distinct angiogenic signals might offer benefit, a concern remains that angiogenesis relapses through compensation by other angiogenic factors. We therefore explored a fundamentally different antiangiogenic strategy.

Targeting endothelial cell (EC) metabolism for antiangiogenesis has received little attention (De Bock et al., 2013a; Harjes et al., 2012). Since angiogenic signaling pathways converge onto metabolism, and ECs rely on glycolysis for generating most (85%) of their ATP (De Bock et al., 2013b), we hypothesized that targeting glycolysis might provide an alternative therapeutic opportunity for reducing pathological neovascularization. However, given that previous antiglycolytic, anticancer therapies were not always successful (Granchi and Minutolo, 2012; Raez et al., 2013), it was unknown if antiglycolytic strategies could inhibit pathological angiogenesis.

We focused on phosphofructokinase-2/fructose-2,6-bisphosphatase-3 (PFKFB3), since silencing in vitro or inactivation in vivo of this glycolytic activator reduced glycolysis and impaired vessel sprouting (De Bock et al., 2013b). This enzyme is an activator of a key glycolytic enzyme, 6-phosphofructo-1-kinase (PFK-1), which converts fructose-6-phosphate (F6P) to fructose-1,6-bisphosphate ($F1,6P_2$). PFKFB isoenzymes synthesize fructose-2,6-bisphosphate ($F2,6P_2$), an allosteric activator of PFK-1 and potent stimulator of glycolysis (Van Schaftingen et al., 1982). Of all PFKFB isoenzymes, PFKFB3 has a much (700-fold) higher kinase than bisphosphatase activity and promotes production of $F2,6P_2$ and glycolysis (Yalcin et al., 2009). PFKFB3 is also the most abundant isoenzyme in ECs (De Bock et al., 2013b). Here, we characterized the antiangiogenic therapeutic potential of a PFKFB3 inhibitor.

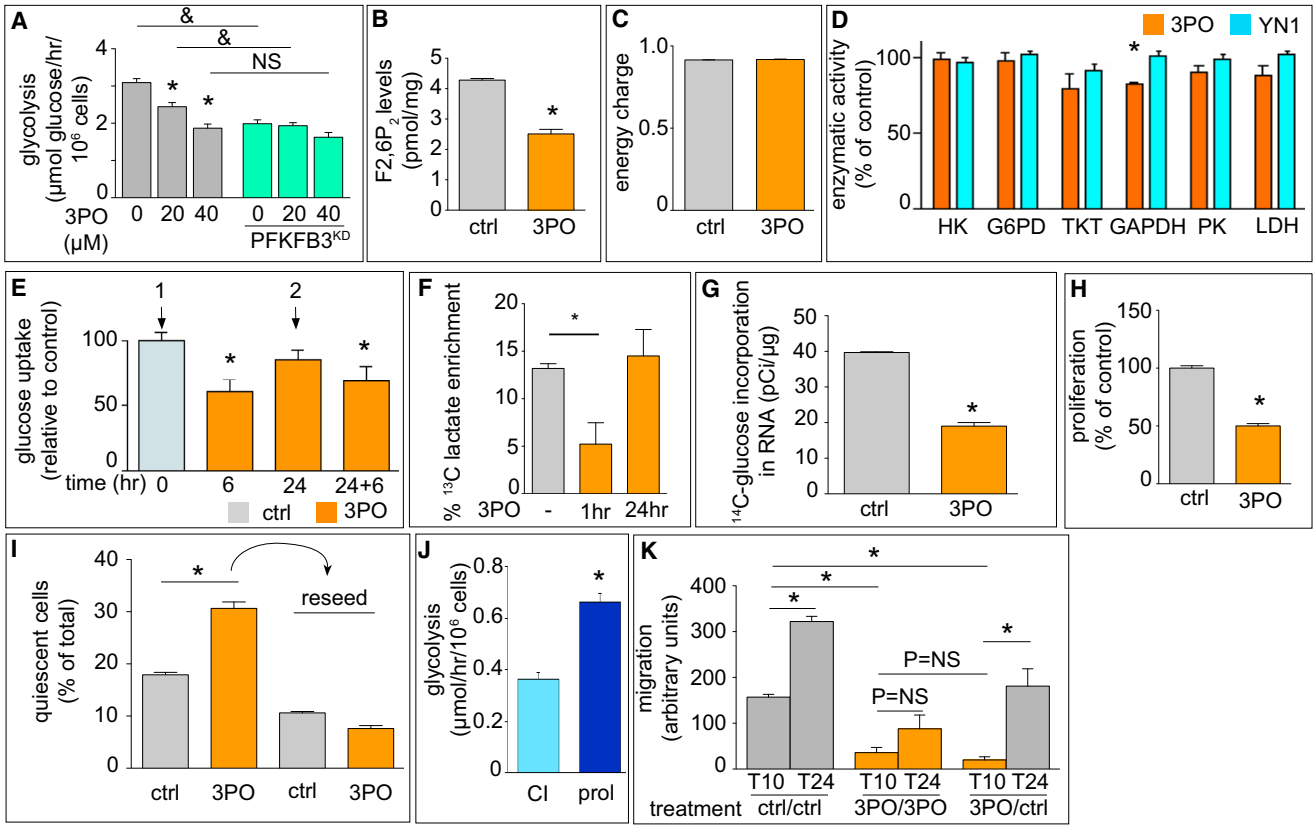

Figure 1. 3PO Inhibits Glycolysis in ECs

(A) Glycolytic flux in control or PFKFB3-silenced ECs, showing that 3PO reduced glycolysis in control cells but was ineffective in further reducing glycolysis in PFKFB3-silenced cells (mean ± SEM; n = 3; *p < 0.05 versus vehicle; &p < 0.05 versus control).

(B) Quantification of fructose-2,6-bisphosphate ($F2,6P_2$) content, showing reduced $F2,6P_2$ levels after PFKFB3 inhibition by 3PO (mean ± SEM; n = 3; *p < 0.05).

(C) PFKFB3 blockade by 3PO did not affect the energy charge ([ATP] + ½[ADP]) / ([ATP] + [ADP] + [AMP]) (mean ± SEM; n = 3; p = not significant [NS]) at 24 hr.

(D) Enzymatic activity of glycolytic enzymes measured in extracts of ECs, treated with a concentration of 3PO or YN1 that effectively inhibited glycolysis, showing that these PFKFB3 blockers failed to affect their enzymatic activity (mean ± SEM; n = 3; *p < 0.05). HK, hexokinase; G6PD, glucose 6-phosphate dehydrogenase; TKT, transketolase; GAPDH, glyceraldehyde 3-phosphate dehydrogenase; PK, pyruvate kinase; LDH, lactate dehydrogenase.

(E) Glucose uptake in vivo, showing that a first injection of 3PO (vertical arrow 1) lowered 2-[1-^{14}C]-DG uptake in the diaphragm modestly and transiently during the first 6 hr, but not after 24 hr. A second administration of 3PO after 24 hr (vertical arrow 2) reduced glucose uptake again to the same level as the first administration (mean ± SEM; n = 3; *p < 0.05).

(F) GC-MS analysis of ^{13}C enrichment in lactate, showing that lactate production from [U-^{13}C]-glucose in the blood was transiently reduced upon 3PO treatment after 1 hr, but not any longer after 24 hr (mean ± SEM; n = 4 for ctrl and n = 5 for 3PO; *p < 0.05 versus vehicle at the same time point).

(G) [6-^{14}C]glucose incorporation assay, showing that 3PO reduced the synthesis of RNA in EC monolayers (mean ± SEM; n = 3; *p < 0.01).

(H) [^{3}H]thymidine incorporation assay, showing that 3PO reduced proliferation of EC monolayers (mean ± SEM; n = 3; *p < 0.01).

(I) FACS quantification of 5-ethynyl-2′-deoxyuridine (EdU^{-}) ECs, showing that 3PO treatment increased the fraction of quiescent ECs. Upon reseeding in the absence of 3PO, ECs reinitiate proliferation (mean ± SEM; n = 3; *p < 0.05).

(J) Glycolytic flux is lower in quiescent ECs (81% ± 3% synchronized in G_0/G_1 by contact inhibition [CI]) than in proliferating (prol) ECs (35% ± 1% in G_0 upon replating) (mean ± SEM; n = 3; *p < 0.05).

(K) Quantification of MitoC-treated EC migration in scratch wound assays over time (10 and 24 hr), showing reduced migration upon PFKFB3 blockade (3PO). When 3PO was removed from the medium 10 hr after the initiation of the treatment, ECs resumed migration (mean ± SEM; n = 3; *p < 0.05). See also Figure S1.

RESULTS

PFKFB3 Blockers Reduce Glycolysis in EC Monolayers In Vitro

To explore if pharmacological blockade of the kinase activity of PFKFB3 reduced glycolysis in human umbilical venous endothelial cells (HUVECs, abbreviated as ECs) and affected vessel sprouting, we used the small molecule compound 3-(3-pyridinyl)-1-(4-pyridinyl)-2-propen-1-one (3PO) (Chesney et al., 1999; Clem et al., 2008). Key findings were confirmed by using 7,8-dihydroxy-3-(4-hydroxyphenyl)-chromen-4-one (YN1), another PFKFB3 blocker (Seo et al., 2011). 3PO and YN1 dose dependently reduced glycolysis in ECs, but by no more than 35%–40% (Figure 1A; Figure S1A available online). 3PO evoked comparable effects in arterial ECs (Figure S1B). PFKFB3 blockade thus reduced glycolysis incompletely, i.e., less than the nonmetabolizable glucose analog 2-deoxy-D-glucose (2DG), which reduced glycolysis by ~80% (Figure S1C). 3PO

also lowered F2,6P_2 levels by 41% (Figure 1B). 3PO, however, did not lower the energy charge (Figure 1C) and, unlike 2DG, did not increase oxygen consumption (Figure S1D).

3PO and YN1 did not inhibit the enzymatic activity of a panel of glycolytic enzymes when analyzing EC lysates (Figure 1D) or purified enzymes (Figures S1E–S1I). When measuring glycolytic flux by using D-[5-^{3}H]-glucose, 3PO did not further reduce glycolysis in ECs in which PFKFB3 was silenced to nearly undetectable protein levels (Figure 1A). YN1 reduced glycolysis in PFKFB3-silenced cells slightly more (Figure S1A), in agreement with its partial effect on PFKFB4 (Seo et al., 2011).

PFKFB3 Blockade Reduces Glycolysis Partially and Transiently In Vivo

We also determined the effect of 3PO on glycolysis in vivo in mice by measuring 2-[1-^{14}C]-deoxy-D-glucose (2-[1-^{14}C]-DG) uptake as an indirect parameter of glycolysis. 3PO lowered 2-[1-^{14}C]-DG uptake by 38% and 41% in the diaphragm and heart, but only transiently during 6 hr (Figure 1E). However, a second administration of 3PO 24 hr later comparably reduced 2-[1-^{14}C]-DG uptake (Figure 1E). Intravenous injection of [U-^{13}C]-glucose and analysis of ^{13}C-lactate enrichment in the blood by gas chromatography-mass spectrometry (GC-MS) confirmed the transient reduction in glycolysis upon 3PO injection (Figure 1F).

PFKFB3 Blockers Reduce EC Proliferation and Migration In Vitro

In EC monolayers, 3PO reduced [6-^{14}C]-glucose incorporation in RNA, a process involving the nonoxidative branch of the pentose phosphate pathway (non-oxPPP) that generates pentoses for nucleotide synthesis (Figure 1G). 3PO also decreased EC proliferation (Figure 1H), in agreement with PFKFB3 silencing data (De Bock et al., 2013b). Instead, 3PO increased the fraction of quiescent ECs (Figure 1I). This effect was reversible, as removal of 3PO restored the fraction of cycling cells (Figure 1I). In accordance, glycolysis was 40% lower in contact-inhibited quiescent ECs than in cycling ECs (Figure 1J). To study EC migration in the absence of confounding effects of proliferation, we treated ECs with mitomycin C (MitoC) to inhibit proliferation. 3PO reduced MitoC-treated EC migration in a scratch wound and modified Boyden chamber assay, and the effects were reversible upon washout of 3PO (Figure 1K; Figure S1J). Similar data were obtained for YN1 (Figures S1K and S1L).

PFKFB3 Blockers Impair Vessel Sprouting In Vitro

To study the effect of PFKFB3 blockers on vessel sprouting, we used EC spheroids. Similar to that in vivo, a tip cell with filopodia-like protrusions takes the lead, while proliferating stalk cells elongate the sprout. PFKFB3 was essential for vessel outgrowth, as both 3PO and YN1 shortened sprout length and decreased sprout numbers (Figures 2A–2D; Figures S2A, S2B, S2D, and S2E), similar to the effect induced by PFKFB3 silencing (De Bock et al., 2013b). 2DG also reduced vessel sprouting (Figures S2C–S2E), but unlike 3PO-treated spheroids that retained a healthy morphology, 2DG-treated spheroids disintegrated and eventually died, as revealed by TO-PRO 3 staining (Figures S2F–S2H), indicating that near-complete inhibition of glycolysis causes cellular demise and death. Counting of Hoechst 33342-stained nuclei revealed that 3PO reduced EC numbers in vascular sprouts (Figures 2E–2G). 3PO also decreased the incorporation of bromodeoxyuridine (BrdU) in spheroid sprout ECs (Figure 2H), indicating that blockade of PFKFB3 impairs sprouting at least partially via reducing EC proliferation. 3PO also impaired EC migration, as it reduced sprouting after MitoC treatment (Figures 2I and 2J). Furthermore, 3PO impeded capillary tube formation (Figures S2I and S2J).

PFKFB3 increases glycolysis but decreases the oxidative pentose phosphate pathway (oxPPP) flux (Herrero-Mendez et al., 2009). This pathway with its rate-limiting enzyme glucose-6-phosphate dehydrogenase (G6PD) generates NADPH, used to reduce oxidized glutathione for antioxidant defense. Notably, 3PO increased the oxPPP flux (Figure 2K) and, consistent with previous reports that the oxPPP promotes angiogenesis (De Bock et al., 2013a; Leopold et al., 2003), blocking the oxPPP by 6-aminonicotinamide (6AN) decreased vessel sprouting (Figures 2L and 2M). However, this increase did not explain the impaired vessel sprouting phenotype by 3PO, since blocking the oxPPP by 6AN did not abrogate the antisprouting activity of 3PO (Figures 2L and 2M). Furthermore, addition of sodium pyruvate at a concentration that increases oxygen consumption (De Bock et al., 2013b) did not rescue the impaired vessel sprouting in 3PO-treated spheroids (Figures S2K and S2L), indicating that diminishing glycolysis by 3PO did not reduce vessel sprouting by diminishing entry of glycolytic intermediates into the tricarboxylic acid (TCA) cycle for oxidative glucose metabolism.

PFKFB3 Blockade Does Not Alter the Expression of Tip- or Stalk-Enriched Genes

We analyzed if PFKFB3 impeded tip or stalk cell formation by reducing the expression of VEGF receptor 2 (VEGFR2) and Dll4, known to influence tip versus stalk cell formation, respectively (Geudens and Gerhardt, 2011; Potente et al., 2011). However, RT-PCR analysis revealed that 3PO did not alter the expression of tip or stalk cell-enriched genes (Figure 2N). Indeed, 3PO did not affect transcript levels of Dll4 or of the Notch1 target genes HES1, HEY1, and HEY2. Expression of VEGFR2 was also not affected by 3PO at the mRNA or protein level (Figure 2N; Figure S2M). Since 2DG interferes with glycosylation by affecting the hexosamine biosynthetic pathway, a side pathway of glycolysis, we examined if 3PO had similar effects. However, VEGFR2 was detected as a fully glycosylated 230 kDa form in 3PO-treated ECs (Figure S2M), suggesting that glycosylation was not impaired. Fluorescence-activated cell sorting (FACS) analysis also failed to reveal a difference in VEGFR2 levels on the cell surface (Figure S2N). Overall, consistent with PFKFB3 loss-of-function studies in ECs (De Bock et al., 2013b), the impaired vessel sprouting by 3PO was not attributable to a change in the expression of tip versus stalk cell signature.

PFKFB3 Blockers Impair Vessel Sprouting in Zebrafish

To explore the functional in vivo relevance of PFKFB3 inhibition, we used *fli1:EGFP^{y1}* zebrafish embryos expressing GFP in ECs and focused on intersomitic vessels (ISVs), which branch off from the dorsal aorta in a ventral-to-dorsal direction and establish the dorsal longitudinal anastomosing vessel (DLAV). We analyzed only viable embryos without developmental defects

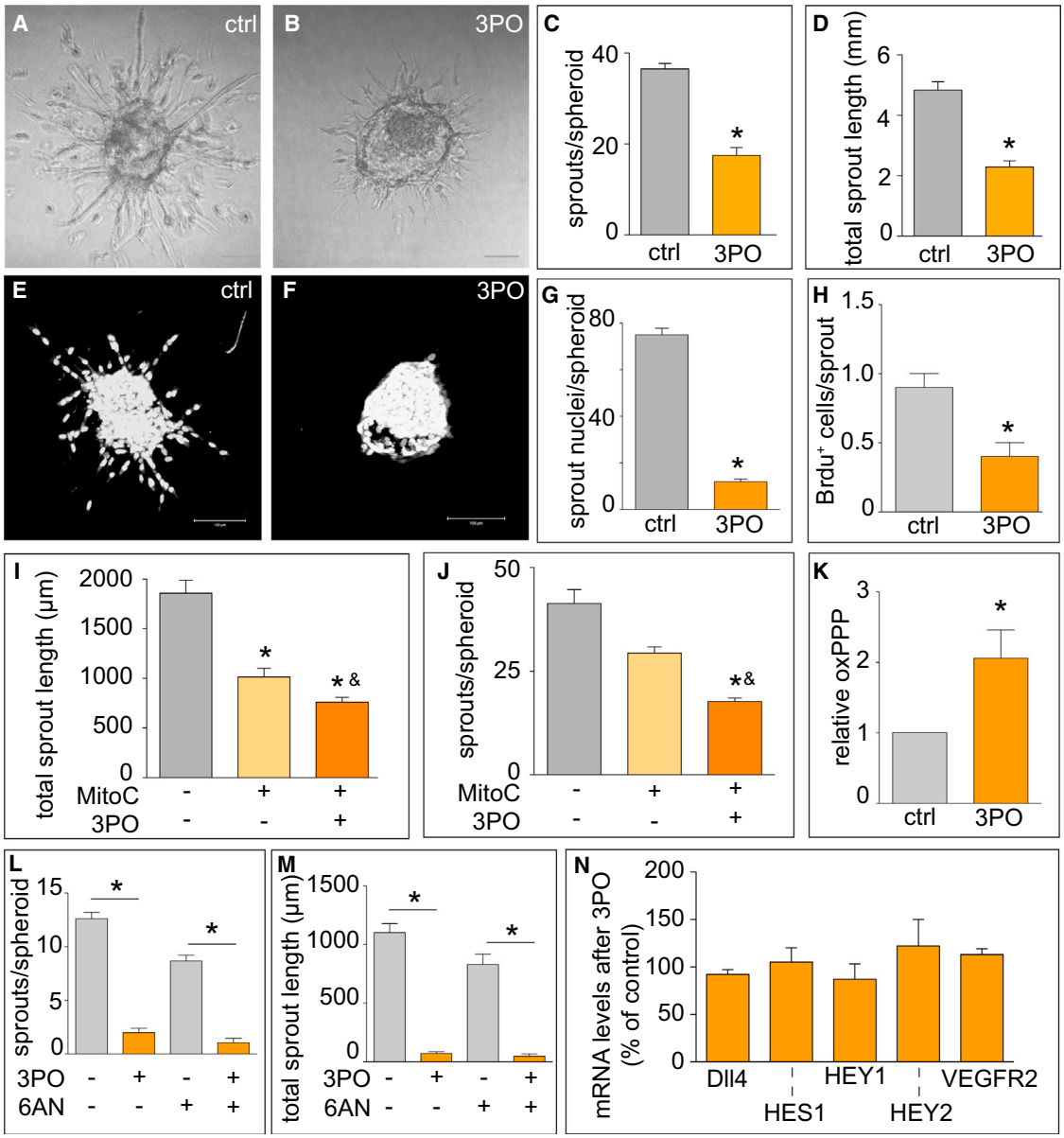

Figure 2. Pharmacological Blockade of PFKFB3 by 3PO Impairs Sprouting In Vitro

(A and B) Representative bright-field micrographs of control (A) and 3PO-treated (B) EC spheroids, showing reduced vascular sprouting in spheroids in the presence of the PFKFB3 inhibitor 3PO (B). Scale bars: 50 µm.

(C and D) Morphometric quantification of EC spheroid sprouting, revealing that blockade of PFKFB3 by 3PO reduced the number of sprouts per spheroid (C) and total sprout length (D) (mean ± SEM; n = 30; *p < 0.01).

(E and F) Representative fluorescence photographs of Hoechst 33342-stained EC spheroids (E), showing a reduced number of EC nuclei in the sprouts of 3PO treated spheroids (F).

(G) Quantification of Hoechst 33342-stained ECs, showing that 3PO treatment reduces the number of nuclei per sprout (mean ± SEM; n = 30 spheroids; *p < 0.001).

(H) Quantification of $BrdU^+$ ECs in spheroid sprouts, showing reduced proliferation upon PFKFB3 blockade by 3PO (mean ± SEM; n = 23 spheroids; *p < 0.005).

(I and J) Morphometric quantification of EC spheroid sprouting, revealing that blockade of PFKFB3 by 3PO reduced the total sprout length (I) and number of sprouts per spheroid (J) even after MitoC-induced mitotic arrest (mean ± SEM; n = 30; *p < 0.05 versus ctrl and $^{\&}$p < 0.05 versus MitoC).

(K) Quantification of oxPPP, showing increased flux upon 3PO treatment (mean ± SEM; n = 4; *p < 0.04).

(L and M) Morphometric quantification of vessel sprouting from EC spheroids upon 6AN treatment, showing that blockade of the oxPPP affects neither the 3PO-induced reduction of the number of sprouts per spheroids (L) nor the total sprout length (M) (mean ± SEM; n = 20; *p < 0.0001).

(N) mRNA expression analysis of DLL4, HES1, HEY1, HEY2, and VEGFR2, showing unaltered expression after PFKFB3 blockade (mean ± SEM; n = 3; p = NS). See also Figure S2.

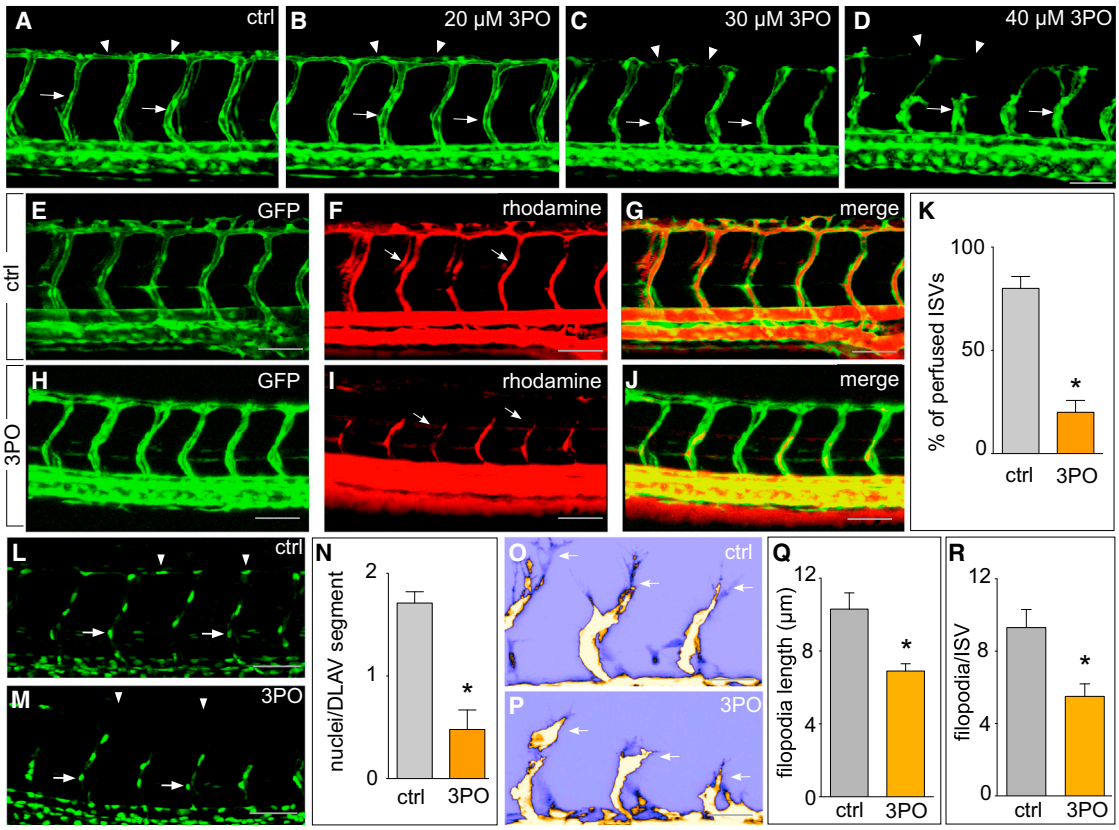

Figure 3. Pharmacological Blockade of PFKFB3 Impairs Vascular Development in Zebrafish Embryos

(A–D) Confocal images of GFP$^+$ vessels in 35 hpf *fli1:EGFP^{y1}* embryos treated with DMSO (ctrl) (A), 3PO (20 μM) (B), 3PO (30 μM) (C), or 3PO (40 μM) (D) from 20 hpf onward, showing impaired outgrowth of ISVs (arrows) and defective formation of the DLAV (arrowheads). Scale bars: 50 μm.

(E–J) Confocal images of 48 hpf *fli1:EGFP^{y1}* embryos after intracardiac angiography with rhodamine-labeled dextran, showing that compared to control embryos, 3PO treatment (40 μM; from 20 hpf onward) reduced ISV perfusion. Control, GFP signal (E); control, rhodamine-dextran signal (F); control, merge (G); 3PO treated, GFP signal (H); 3PO treated, rhodamine-dextran signal (I); 3PO treated, merge (J).

(K) Quantification of perfused ISVs in *Tg(kdrl:EGFP;gata1:DsRed)* zebrafish (mean ± SEM; n = 3 for control and n = 4 for 3PO; *p < 0.001).

(L–N) Confocal images of GFP$^+$ vessels in 35 hpf *fli1:nEGFP^{y7}* zebrafish embryos treated with DMSO (ctrl) (L) or 3PO (40 μM) (M) from 20 hpf onward, showing that 3PO reduced EC numbers in the ISVs (arrows) and in the DLAV (arrowheads), and quantification (N) (mean ± SEM; n = 8 for control and 6 for 3PO; *p < 0.0001).

(O and P) Pseudocolor lookup table (LUT) high-magnification confocal images of GFP$^+$ ISVs in 35 hpf *fli1:EGFP^{y1}* zebrafish embryos showing that compared to controls (O), embryos treated with 3PO (45 μM) have fewer and shorter filopodia (P).

(Q and R) Quantification of the filopodia length (Q) and number (R) (filopodia length: n = 30 for ctrl and n = 20 for 3PO; *p < 0.0001; filopodia number per ISV: n = 4; *p < 0.005). See also Figure S3 and Movie S1.

and with an intact circulation (Figure S3A–S3D). When treating embryos with 3PO from 20 hr postfertilization (hpf) onward, just prior to the onset of ISV sprouting, 3PO dose dependently impaired ISV sprouting (Figures 3A–3D). At 40 μM, only <5% of the embryos formed ISVs, but these vessels had perfusion defects (see below). Time-lapse video imaging of 3PO-treated embryos showed that the ISVs failed to grow out normally and established only an incomplete DLAV (Movie S1). At the highest concentration of 3PO (40 μM), a fraction of ISVs stalled midway, exhibiting blunt ends without side branches or anastomoses, and failed to form a DLAV (Figure 3D). Withdrawal of 3PO reinitiated branching, showing that 3PO did not cause irreversible EC demise (Figures S3E–S3G). Similar results were obtained for YN1 (Figures S3H–S3J). Angiography after intracardiac injection of rhodamine-labeled dextran showed that 3PO reduced the number of perfused ISVs (Figures 3E–3J). Analysis of *Tg(kdrl:EGFP;GATA1:DsRed)* zebrafish, in which vessels are GFP$^+$ and erythrocytes are DsRED$^+$, confirmed these findings (Figure 3K).

Counting of EC nuclei in *fli1:nEGFP^{y7}* zebrafish embryos, expressing GFP in endothelial nuclei, showed that 3PO decreased EC numbers in the DLAV (Figures 3L–3N). In addition, time-lapse video imaging revealed that 3PO altered the leading edge of the vascular front, where tip cells reside. In contrast to the rapidly advancing and dynamically exploring vascular front in control embryos, tip cells in 3PO-treated embryos were less dynamic and exploratory and moved more slowly, almost creeping forward (Movie S1). In control embryos, tip cells were polarized in a rear-to-front direction, often projecting at the leading edge two to three "foot-like" cytosolic protrusions (2–3 μm wide) from where multiple, rapidly moving, and highly motile long filopodia extended (Figures 3O–3R). By contrast, in 3PO-treated embryos, tip cells projected shorter, thinner, and more blunt-ended "foot-like"

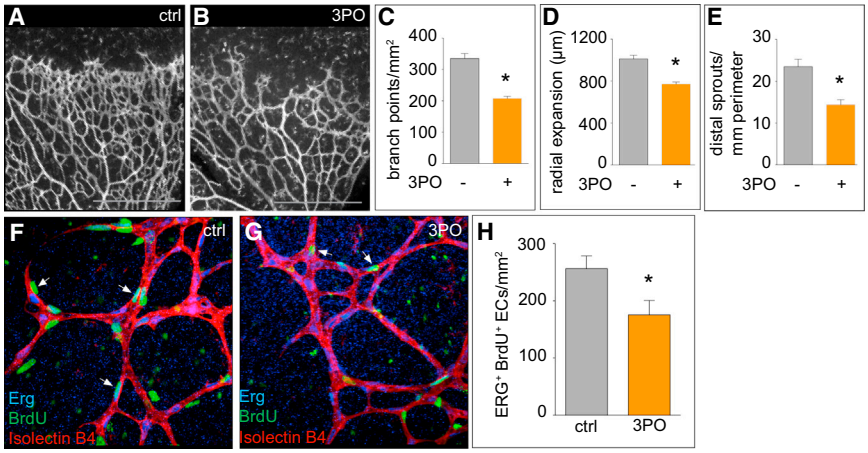

Figure 4. Pharmacological PFKFB3 Blockade Impairs Vascular Development in Mice

(A and B) Confocal images of isolectin-B4-stained (gray) retinal vessels of postnatal day 5 (P5) pups at high magnification, showing, as compared to DMSO-treated mice (A), reduced vascular branching in 3PO-treated mice (50 mg/kg) (B). Scale bars: 50 μm.

(C–E) Quantification of the effect of 3PO treatment on the number of branch points (C), radial expansion (D), and the number of distal sprouts with filopodia (E) in the retinal vasculature of 3PO-treated mice (mean ± SEM; n = 3 for ctrl and n = 5 for 3PO; *p < 0.001).

(F and G) Triple staining for Erg (blue), isolectin B4 (red), and BrdU (green) at the vascular front of the retinal plexus of control (F) and 3PO-treated (G) mice confirmed that EC proliferation was reduced in 3PO-treated mice (G) (mean ± SEM; n = 3; p < 0.05). Arrows: proliferating ECs.

(H) Quantification of $BrdU^+$ Erg^+ cells/mm^2 retinal area, revealing lower proliferation of retinal ECs after 3PO treatment (mean ± SEM; n = 3; *p < 0.05). Scale bars: 50 μm. See also Figure S4.

cytosolic protrusions and extended fewer and shorter filopodia (Figures 3O–3R).

PFKFB3 Blockers Impair Vessel Sprouting in the Mouse Retina

We also studied the effects of PFKFB3 blockade on vascular sprouting in the postnatal retina, a widely used mouse model to characterize tip and stalk cell phenotypes. Treatment of pups with 3PO at postnatal days 1–4 (P1–P4) reduced the number of branch points (Figures 4A–4C), the radial expansion of the vascular plexus (Figure 4D), and the number of distal sprouts with filopodia (Figure 4E). YN1 also reduced vessel branching in the retina (Figures S4A–S4D). Staining of retinal flat mounts for isolectin B4, BrdU, and Erg (an EC-specific nuclear transcription factor) revealed that fewer Erg^+ $BrdU^+$ ECs were present in the vascular plexus in 3PO-treated mice, suggesting that EC proliferation was impaired (Figures 4F–4H). Confirming the gene expression data in EC monolayers, 3PO did not affect the expression of the tip cell-enriched marker *Pdgfb* in retinal tip cells (Figures S4E and S4F).

Blocking PFKFB3 Inhibits Vascular Hyperbranching

We then explored if PFKFB3 blockade counteracted vascular hyperbranching. VEGFR1 (Flt1) is an inhibitor of vascular branching and, consistent with previous findings (Krueger et al., 2011), *flt1* knockdown ($flt1^{KD}$) caused ISV hyperbranching (Figures 5A and 5B). 3PO normalized ISV hyperbranching in a large fraction of $flt1^{KD}$ embryos and reduced the severity of vascular overgrowth (Figures 5C and 5D). While 64% of control-treated $flt1^{KD}$ embryos exhibited signs of severe ISV hyperbranching in at least 4 out of 10 ISVs per embryo, only 20% of 3PO-treated $flt1^{KD}$ embryos showed this phenotype, and up to 29% of them formed completely normal ISVs. 3PO also reduced ISV side branches in $flt1^{KD}$ embryos (side branches per ISV: 100% ± 10% for $flt1^{KD}$ controls versus 54% ± 10% for 3PO-treated $flt1^{KD}$; n = 3 experiments, each with >8 embryos per condition; $p < 0.01$ by univariate test). We also analyzed ISV perfusion. In control embryos, intracardiac angiography with rhodamine-labeled dextran showed that PFKFB3 blockade impaired vessel lumen formation and perfusion (see above). In contrast, ISVs in Flt1-silenced ($flt1^{KD}$) embryos had an enlarged lumen, but PFKFB3 blockade largely normalized ISV lumen size in $flt1^{KD}$ embryos (Figures S5A–S5F) without impairing vessel perfusion (Figure S5G).

We also induced vascular hyperbranching by blocking Dll4/Notch signaling (Hellström et al., 2007). In EC spheroids, N-(N-(3,5-Difluorophenacetyl)-L-alanyl)-S-phenylglycine t-butyl ester (DAPT) increased the number and length of the vessel sprouts, but this hypersprouting was abrogated by 3PO (Figures S5H–S5K). 3PO also rescued vascular hyperbranching in zebrafish embryos upon silencing of Dll4 (Figures S5L–S5O) or in the retina upon treatment of neonatal mice with DAPT (Figures 5E–5H).

PFKFB3 Blockade Amplifies the Antiangiogenic Effect of VEGFR Blockers

VEGF blockade is a clinically approved antiangiogenic strategy. The VEGFR tyrosine kinase inhibitor SU5416 caused dose-dependent vascular defects in zebrafish embryos, characterized by progressive impairment and stalling of ISVs and lack of DLAV formation. At a maximal concentration (1 μM), SU5416 prevented the outgrowth of ~30% of the ISVs (Figure 5I). These defects were not only more severe, but also occurred at a higher incidence when increasing the dose of SU5416 (Figure 5I).

To evaluate if PFKFB3 blockade enhanced the antiangiogenic effect of VEGFR inhibition, we treated embryos with suboptimal doses of SU5416 (0.1 or 0.5 μM) and 3PO (20 or 30 μM), which alone only induced a negligible impairment of ISV outgrowth in a minority of embryos (Figures 5J–5L). However, the combination of both compounds at suboptimal doses aggravated the vessel defects in most embryos (Figures 5I and 5M). Even when a high dose of SU5416 (1 μM) was used that prevented the formation of half of the ISVs, the combination with 3PO (30 μM) further aggravated this phenotype, abrogating ISV development in nearly all embryos (Figure 5I). Overall, blockade of glycolysis amplified the efficacy of targeted VEGF inhibition in blocking angiogenesis.

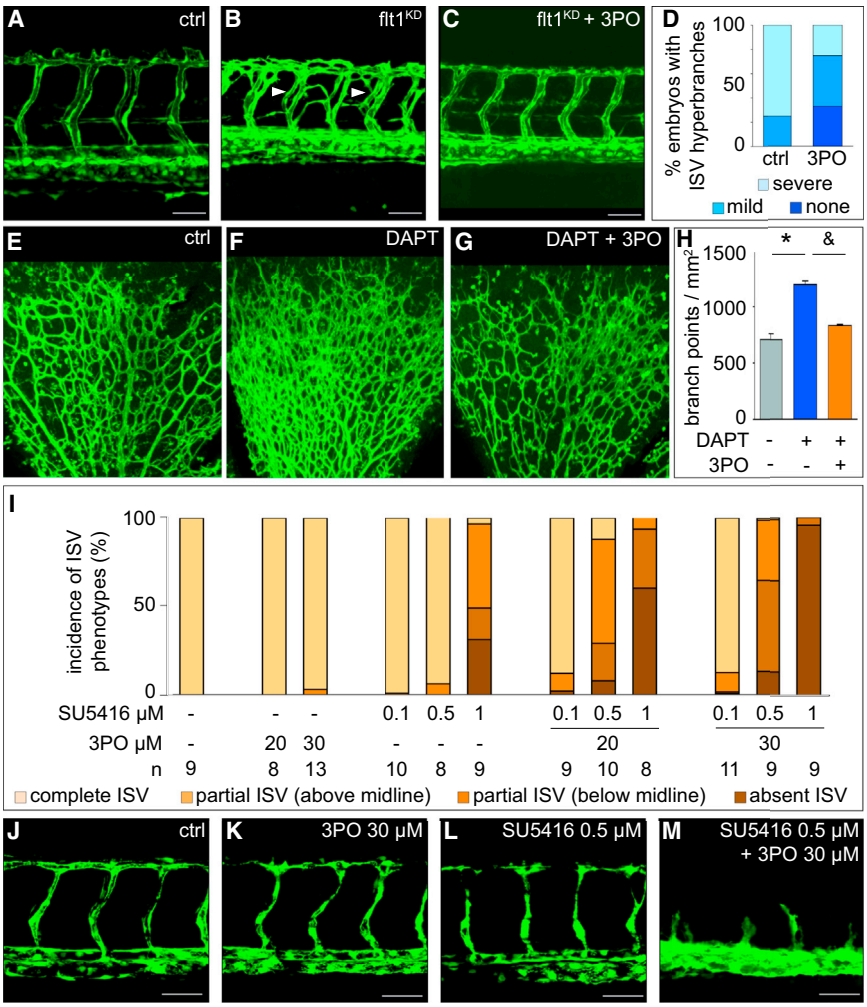

Figure 5. PFKFB3 Blockade Inhibits Vascular Hyperbranching In Vivo

(A–D) Confocal images of 72 hpf *fli1:EGFP*^{y1} embryos. As compared to the normally patterned ISV in a control embryo (A), ISVs hyperbranch in *flt1*^{KD} embryos (arrowheads in B). Treatment of *flt1*^{KD} embryos with 3PO (30 µM) largely normalized the vascular hyperbranching phenotype (C). Shown in (D) is the incidence of *flt1*^{KD} embryos with no, mild, or severe vascular hyperbranching, revealing that 3PO reduced vascular hyperbranching (n = 12; *p < 0.00001). Scale bars: 50 µm.

(E–G) Confocal images of the retinal vasculature after treatment with control (E), DAPT (F), or DAPT + 3PO (G), showing that DAPT increased the number of branch points and that 3PO abolished the hyperbranching induced by DAPT.

(H) Quantification of the number of branches (mean ± SEM; n = 5 for DAPT and 3PO+DAPT, n = 8 for ctrl; *p < 0.001 versus control (gray), &p < 0.05 versus DAPT).

(I) Quantification of the average incidence of indicated ISV phenotypes for 10 ISVs scored per embryo upon single or combined treatment with the indicated doses of 3PO and/or SU5416. Complete ISV, ISVs formed normally and completely; partial ISV (above midline), ISVs formed at least until or partially above the horizontal midline without reaching the dorsal roof level; partial ISV (below midline), ISVs were severely underdeveloped and failed to reach the horizontal midline; absent ISV, ISVs completely failed to sprout. n values per condition are indicated under the bars.

(J–M) Confocal images of GFP$^+$ vessels in 35 hpf *fli1:EGFP*^{y1} embryos, showing a control embryo (J) and a minor impairment of ISV development when treating embryos with a submaximal dose of 3PO (K) or the VEGFR tyrosine kinase inhibitor SU5416 (L) but severe vascular defects and near-complete abrogation of ISV formation in embryos treated with the combination of both inhibitors (M). Scale bars: 50 µm. See also Figure S5.

Blockade of PFKFB3 Reduces Pathological Angiogenesis

We tested if PFKFB3 blockade inhibited choroidal neovascularization (CNV), a model of age-related macular degeneration (AMD) (Van de Veire et al., 2010). The lesions in this model are largely vascular in nature, allowing us to assess antiangiogenic effects of 3PO. Starting from 1 day after laser burn injury of the Bruch's membrane to induce CNV, mice received a daily dose of vehicle or 3PO. Quantification of CNV lesions upon injection with fluorescein isothiocyanate (FITC)-conjugated dextran at 14 days after laser injury showed that 3PO dose dependently reduced the CNV lesion volume (Figures 6A–6C). We also evaluated if 3PO amplified the antiangiogenic activity of the anti-VEGFR2 monoclonal antibody (mAb) DC101 (Van de Veire et al., 2010). When using a suboptimal dose of DC101 (12.5 mg/kg, 3× per week), CNV was reduced by 38%, while the combination of DC101 plus 3PO caused a decrease of CNV by 67% (Figure 6D).

We confirmed the antiangiogenic activity of 3PO by using other models of pathological angiogenesis. We first used the oxygen-induced model of retinopathy of prematurity (ROP), which is based on the exposure of mouse pups to hyperoxia during a phase when their retinal vasculature is still developing, from P7–P12. This causes capillary depletion and vascular rarefication and, upon return to room air, results in retinal ischemia and, subsequently, in the formation of proliferative vascular tufts by P17–P21 (Scott and Fruttiger, 2010). Like in CNV, the lesions in the ROP model are primarily vascular in nature. Treatment of pups with 3PO during the phase of vascular proliferation from P12 to P17 reduced the formation of vascular tufts at P17 (Figures 6E–6G).

We also used two inflammation models, e.g., a skin psoriasis model and an inflammatory bowel disease model, since inflammatory disorders are characterized by increased angiogenesis (Wynn et al., 2013). A previous study reported that 3PO treatment reduced skin epithelial hyperplasia and inflammation, induced by local application of the immune activator imiquimod (IMQ), but this study did not analyze the effects on angiogenesis (Telang et al., 2012). Confirming previous findings, 3PO reduced the epidermal hyperplasia (Figure S6A), the spleen weight, another measure of inflammation (Figure S6B), and the number of CD3$^+$ lymphocytes in the lesions (Figure S6C). Importantly, 3PO also decreased the density of CD105$^+$ vessels in the epidermal lesions (Figures 7A–7D).

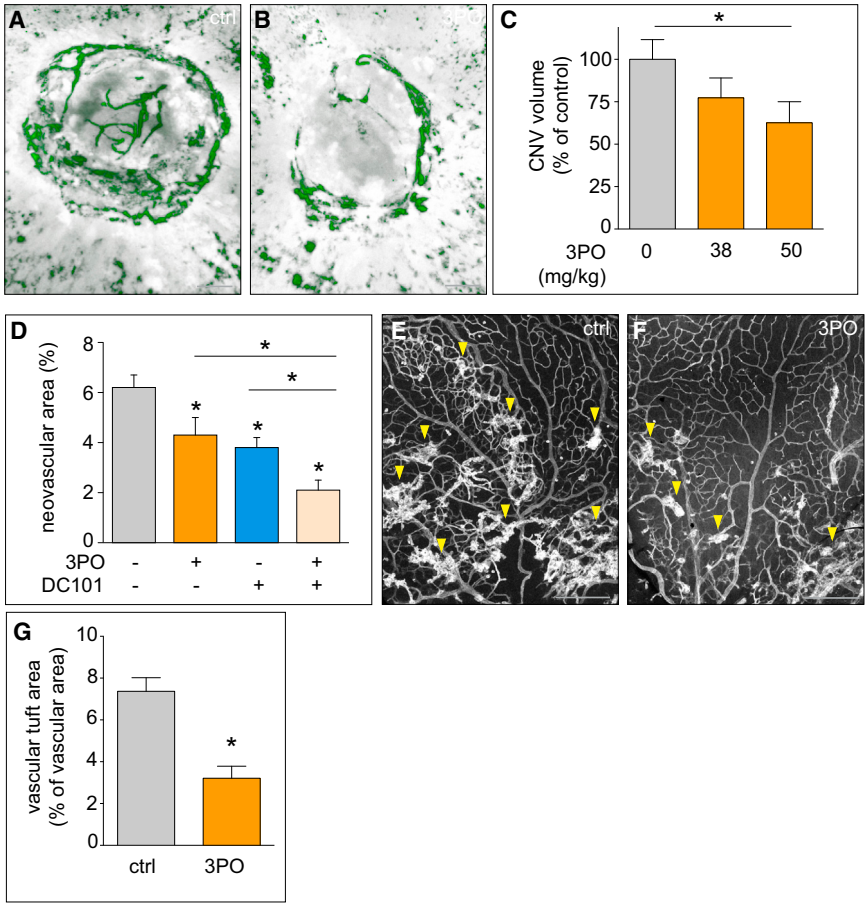

Figure 6. Blockade of PFKFB3 Reduces Pathological Angiogenesis: Ocular Models

(A and B) FITC-dextran choroidal flatmounts of control (A) or 3PO-treated mice (B), revealing fewer choroidal neovessels after 3PO treatment (B). The images are 3D isosurface renderings from z stacks of all individual optical sections through the neovascular lesion, as made by confocal laser scanning microscopy. Scale bars: 50 μm.

(C) 3PO dose dependently reduced CNV volume (estimated marginal mean ± SEM; n = 16 for ctrl, n = 16 for 38 mg/kg 3PO, and n = 14 for 50 mg/kg 3PO; two independent experiments; *p < 0.04 by general linear model univariate analysis, considering experiment as covariate).

(D) The combination treatment of 3PO (50 mg/kg) plus a submaximal dose of the anti-VEGFR2 mAb DC101 reduced the CNV neovascular area more than each monotherapy alone (mean ± SEM; n = 18 for ctrl, n = 7 for 3PO, n = 9 for DC101, and n = 8 for 3PO+DC101; *p < 0.05 versus ctrl or as indicated).

(E and F) Retinal flatmounts of ROP mice treated with DMSO (E) or 3PO (F) (70 mg/kg) and stained for isolectin B4, revealing reduced formation of vascular tufts (arrowheads) after 3PO (70 mg/kg) (F). Scale bars: 50 μm.

(G) Quantification of the vascular tuft area (mean ± SEM; n = 11 for ctrl, n = 9 for 3PO; *p < 0.001).

Inflammatory bowel disease, induced by administration of dextrane sulfate sodium (DSS), is also characterized by pathological angiogenesis (Hindryckx et al., 2010). Quantification of the disease activity index (DAI), which scores body weight loss, stool consistency, and blood in the stool and anal region, revealed that 3PO reduced disease severity (Figure 7H). Hematoxylin and eosin staining (H&E) showed that 3PO-treated mice had less-severe acute colitis (Figures 7E–7G). To quantify the histological signs of colitis, we used a histologic scoring method, taking into account the severity of inflammatory cell infiltration (dispersed, focal, or widespread), the extent of injury (mucosal, submucosal, or transmural), and crypt damage (basal, luminal, or entire crypt loss) (Cummins et al., 2008). This analysis confirmed that 3PO reduced the severity of colitis (histological score, median value: 10 for control versus 6 for 3PO; n = 11 for control and n = 10 for 3PO; p = 0.0004), and decreased $CD45^+$ cell infiltration in the (sub)mucosa and muscularis externa (Figure 7I). 3PO also decreased the area of $CD105^+$ vessels in the inflamed mucosa, submucosa, and muscularis externa (Figures 7J–7M).

DISCUSSION

Glycolysis: An Overlooked Target in Angiogenesis?

ECs rely on glycolysis and derive up to 85% of their ATP from glycolysis, while PFKFB3-driven glycolysis regulates EC proliferation and migration (De Bock et al., 2013b). We now also show that ECs increase glycolysis when shifting from quiescence to proliferation and migration. Glycolysis is required for cell proliferation, not only by providing ATP, but also by generating glycolytic intermediates that are used for the synthesis of macromolecules necessary for cell mass duplication during division (Lunt and Vander Heiden, 2011). In addition, glycolysis is required for EC motility, in part by compartmentalizing PFKFB3 and other glycolytic enzymes in lamellipodia and by concentrating these glycolytic enzymes with F-actin at leading membrane ruffles (De Bock et al., 2013b). The high glycolytic flux in ECs, their dependence on this pathway to generate most of the ATP, and the increased glycolysis during EC proliferation and migration, together with the genetic findings that loss of PFKFB3 in ECs affects tip and stalk cells (De Bock et al., 2013b), render glycolysis an attractive target for therapeutic inhibition of angiogenesis.

PFKFB3 Blockade Reduces Physiological and Pathological Angiogenesis

We previously reported that genetic silencing of PFKFB3 reduces vessel formation in physiological conditions (De Bock et al., 2013b), but it remained untested if pharmacological blockade of PFKFB3 could also impair pathological angiogenesis. 3PO phenocopied the effects of PFKFB3 silencing in ECs in vitro and of PFKFB3 inactivation in ECs in vivo (De Bock et al., 2013b). Indeed, 3PO impaired vessel sprouting in EC spheroids by reducing EC proliferation and migration, impeded filopodia formation, and EC accumulation in ISVs in zebrafish and caused vascular hypobranching and outgrowth in the

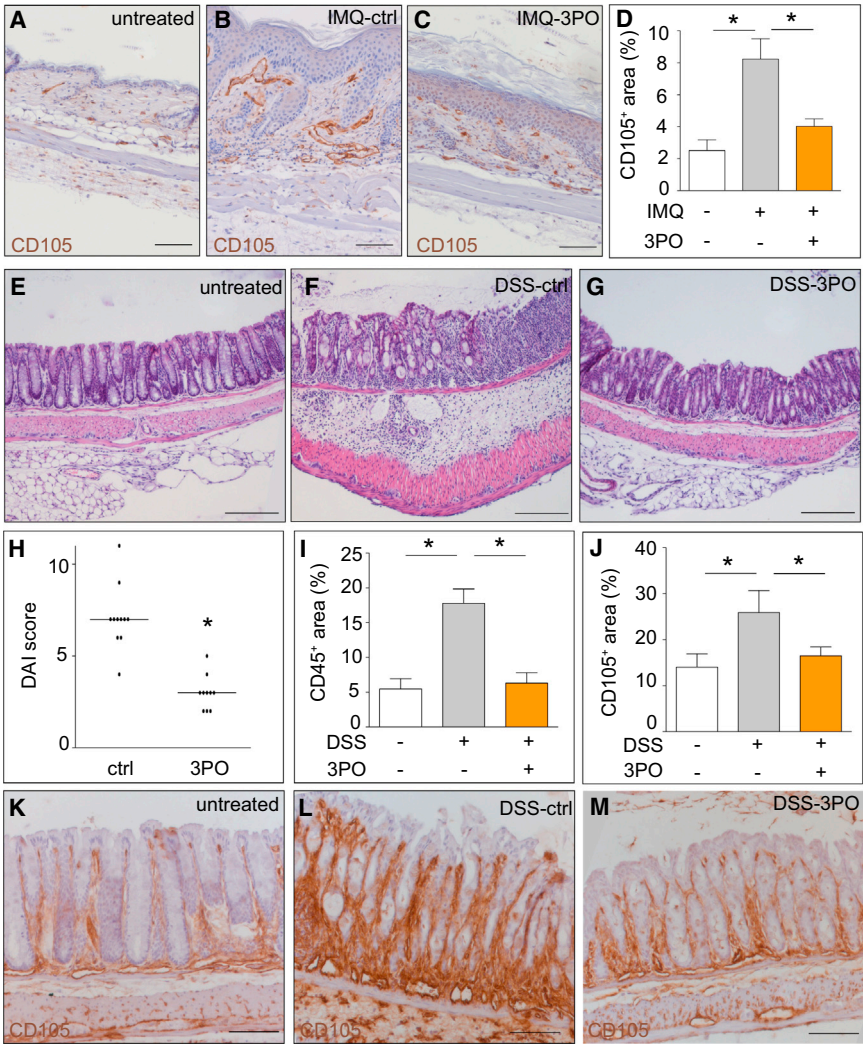

Figure 7. PFKFB3 Blockade Reduces Pathological Angiogenesis: Inflammation Models

(A–C) Representative images of CD105 staining of untreated skin (A), IMQ-DMSO-treated skin (ctrl) (B), and IMQ-3PO-treated skin (3PO) (C). Scale bars: 100 μm.

(D) Reduced CD105$^+$ vascular area in the dermis upon 3PO treatment (mean ± SEM; n = 7 for untreated, n = 9 for IMQ-DMSO and IMQ-3PO; *p < 0.001).

(E–M) DSS-induced colitis model. Representative H&E images of untreated healthy colon (E), DSS-DMSO-treated colon (DSS-ctrl) (F), and DSS-3PO-treated colon (50 mg/kg) (G). Scale bars: 200 μm. (H) Reduced disease activity index (DAI) score upon 3PO treatment (median; n = 11 for DSS-DMSO, n = 10 for DSS-3PO; *p < 0.0001). (I) Reduced CD45$^+$ area in the mucosa, submucosa, and muscularis externa of the colon upon 3PO treatment (mean ± SEM; n = 3 for untreated, n = 11 for control, and n = 10 for 3PO; *p < 0.003). (J) Reduced CD105$^+$ vascular area in the mucosa, submucosa, and muscularis externa of the colon upon 3PO treatment (mean ± SEM; n = 3 for untreated, n = 11 for DSS-DMSO, and n = 10 for DSS-3PO; *p < 0.004). Representative images of CD105 staining of untreated healthy colon (K), DSS-DMSO-treated colon (DSS-ctrl) (L), and DSS-3PO-treated colon (M). Scale bars: 100 μm. See also Figure S6.

mouse retina by decreasing EC proliferation and tip cell behavior. The finding that 3PO impaired lumen formation (a process requiring actin cytoskeleton changes; Sacharidou et al., 2012) is in agreement with findings that PFKFB3 regulates actin cytoskeleton remodeling processes (De Bock et al., 2013b).

3PO also reduced vascular hyperbranching induced by inhibition of Notch or VEGFR1 signaling in zebrafish embryos. In addition, 3PO largely normalized vascular hypersprouting in EC spheroids and the mouse retina, induced by the Notch signaling blocker DAPT. Moreover, 3PO reduced pathological neovascularization in ocular and inflammatory models in the mouse and amplified the antiangiogenic activity of a VEGF receptor tyrosine kinase inhibitor and anti-VEGF receptor 2 in the zebrafish and CNV mouse model, respectively. Together, inhibition of PFKFB3 by 3PO reduces vessel formation in physiological and pathological conditions in the models tested.

Partial and Transient Reduction of Glycolysis

Previous antiglycolytic anticancer strategies attempted to block glycolysis completely and permanently, but these approaches also caused adverse effects (Granchi and Minutolo, 2012). In agreement, our 2DG experiments show that more complete, sustained inhibition of glycolysis induces toxic effects in cultured ECs. In contrast, 3PO reduced glycolysis only partially, inducing EC quiescence without causing EC death in vitro. Likewise, 3PO reduced glycolysis only partially and transiently in vivo, but without inducing permanent refractoriness, since a second 3PO administration 24 hr later reduced glycolysis again to the same level as the first treatment. Thus, a partial and daily transient decrease of glycolysis sufficed to suppress pathological neovascularization. It remains to be studied whether 3PO treatment in vivo has acceptable tolerability.

The transient effect of 3PO is in agreement with its short half-life (30 min), rapid clearance (2,312 ml/kg/min), low Cmax (113 ng/ml) and low area under the concentration-time curve from zero to infinity ($AUC_{0\text{-inf}}$; 36 ng/hr/ml) ($AUC_{0\text{-inf}}$ refers to the actual body exposure to 3PO after administration of a dose of 3PO) (Clem et al., 2013). With the concentrations used, 3PO blocked PFKFB3 completely, since 3PO failed to further reduce glycolysis in ECs in which PFKFB3 was silenced to nearly undetectable levels. Despite full blockade of PFKFB3, glycolysis was only decreased by 35%–40%. Similar data were obtained when silencing PFKFB3 (De Bock et al., 2013b). The reason for the partial effect likely relates to the fact that 3PO blocks an activator of a key enzyme in glycolysis (e.g., PFK-1). Hence, PFKFB3 blockade has a ceiling level in its ability to inhibit glycolysis.

PFKFB3 Blockade: A Different Therapeutic Antiglycolytic Paradigm

Past antiglycolytic therapies faced challenges of cross-inhibition of other glycolytic targets, off-target effects, poor membrane permeability, and inability of compounds to efficiently antagonize abundant glycolytic substrates (Granchi and Minutolo, 2012). For instance, 2DG must compete with mM levels of glucose in the blood, necessitating delivery of high (toxic) amounts (Granchi and Minutolo, 2012). Nonetheless, cancer patients receiving 2DG had a progressive disease and suffered adverse effects (Granchi and Minutolo, 2012; Raez et al., 2013). Some of the side effects were attributed to the fact that these strategies block not only glycolysis, but also other glucose metabolism pathways (Granchi and Minutolo, 2012). Another reason is that these approaches inhibit glycolysis nearly completely and permanently, inducing ATP depletion and toxicity (Granchi and Minutolo, 2012). Indeed, human genetic studies reveal that a decrease in glycolysis due to hereditary mutations in glycolytic genes is well tolerated, as long as the decreased glycolysis levels do not deplete ATP levels (Climent et al., 2009).

PFKFB3 blockade by 3PO differs from these antiglycolytic approaches in various aspects. Firsty, it inhibits a defined intracellular enzyme, requiring much lower (μM) inhibitor concentrations than the high (mM) concentrations of 2DG needed to compete with the mM plasma glucose levels (François et al., 1987). Second, unlike 2DG and related drugs, which block glucose metabolism high up in the pathway, PFKFB3 blockade inhibits a defined downstream target, which specifically reduces glycolytic flux, without abrogating glycolytic side pathways such as the oxidative PPP (oxPPP), necessary for the production of NADPH to secure redox homeostasis. In fact, 3PO increased the oxPPP flux, but this change did not explain the antiangiogenic activity of 3PO. Third, 3PO and YN1 did not inhibit other glycolytic enzymes, tested by using recombinant enzymes or 3PO-treated EC extracts. Fourth, the K_M of PFKFB3 for its substrate fructose-6-phosphate (F6P) is 97 μM, while the K_i for competitive inhibition by 3PO is 25 μM, and 3PO has no effect on PFK-1, which shares an identical substrate, F6P (Clem et al., 2008). Fifth, 3PO did not cause EC death.

3PO Blocks Hyperglycolysis during EC Proliferation and Migration

Of the maximal amount of glycolysis that ECs can generate, they use 40% to proliferate and migrate, reserving 60% for maintenance homeostasis, in line with findings that proliferation only requires 30% of ATP production (Locasale and Cantley, 2010). Lowering glycolysis by 40% through 3PO treatment impaired EC proliferation and migration. This, however, did not cause EC death, but promoted reversible quiescence. PFKFB3 blockade thus reduced the hypermetabolism that is induced when ECs switch from quiescence to proliferation and migration.

Possible Medical Implications

PFKFB3 blockade decreased pathological angiogenesis in inflammatory and ocular disease models. Choroidal neovascularization (a preclinical model of wet AMD) and retinopathy of prematurity are blinding disorders, caused by excessive growth of retinal vessels (Cavallaro et al., 2013; Miller et al., 2013; Stewart, 2012). Anti-VEGF therapy has beneficial effects in AMD and ROP patients, but does not attain durable treatment-free cessation of the disease (Darlow et al., 2013; Niranjan et al., 2012; Rofagha et al., 2013). In addition, one-third of patients with wet AMD have poor visual outcome, and ~13% lost more vision after intraocular anti-VEGF treatment (Lalwani et al., 2009). Our findings that 3PO reduces vascular lesions in both ocular disorders and enhances the antiangiogenic effect of the anti-VEGFR2 in the CNV model may warrant further study of a possible therapeutic use of PFKFB3 blockers.

EXPERIMENTAL PROCEDURES

More detailed methods are described in the Supplemental Experimental Procedures.

Cellular Assays

Freshly isolated primary HUVECs were used for evaluation of metabolism, proliferation, migration, matrigel assay, spheroid capillary sprouting assays, and cell cycle status. Except for Figure 1A, we used the maximal concentration of 3PO that reversibly impaired in vitro EC responses, ranging between 15 and 20 μM.

RNA Expression Analysis

RNA expression analysis was performed by TaqMan qRT-PCR or in situ hybridization.

Metabolism Assays

Glycolysis, glucose incorporation into RNA, and oxidative pentose phosphate pathway flux were determined by incubating cells with radioactive-labeled tracer glucose. Briefly, ^3H_2O formation was a measure for glycolytic flux. $^{14}CO_2$ production was a measure for oxidative pentose phosphate pathway flux, and ^{14}C counts in isolated RNA was a measure for glucose incorporation. Fructose-2,6-bisphosphate levels in cell lysates were determined as described (Van Schaftingen et al., 1982). Oxygen consumption and lactate production were measured using the Seahorse XF24 analyzer. Energy balance was calculated as ([ATP] + ½[ADP]) / ([ATP] + [ADP] + [AMP]) based on high-performance liquid chromatography (HPLC) measurement of AMP, ADP, and ATP levels in cell extracts.

Proliferation

Proliferation was quantified by incubating cells with [^{3}H]-thymidine. The amount of [^{3}H]-thymidine incorporated into DNA was measured by scintillation counting.

Migration

Migration was evaluated using scratch wound or Boyden chamber migration assays. To evaluate responses in the absence of proliferation, MitoC-treated ECs (0.5–1 μg/ml for 24 hr) were used.

Spheroid Capillary Sprouting Assay

ECs were incubated overnight in hanging drops to form spheroids, embedded in collagen, and cultured for 24 hr (with addition of compounds as indicated) to induce sprouting. Cultures were fixed with 4% paraformaldehyde (PFA) and analyzed.

Matrigel Assay

ECs were plated on top of polymerized Matrigel Basement Membrane Matrix in M119 full medium containing 3PO or vehicle. After 6 hr, the network was fixed using 4% PFA.

Cell Cycle Analysis

Cell cycle analysis was determined by flow cytometry based on the DNA and RNA content as stained for with Hoechst and Pyronin Y.

In Vivo Metabolism

Glycolytic flux in vivo was assessed by mass spectrometry detection of ^{13}C-lactate in the plasma, collected 10 min after tail vein injection of [U-^{13}C] glucose. Glucose uptake in vivo was assessed by measuring the radiolabel content of the heart and diaphragm, harvested 1 hr after intravenous bolus injection of the mice with 2-deoxy-D-glucose, 2-[1-^{14}C].

Angiogenesis Models

Zebrafish

Tg(fli1:EGFP)^{y1} or *Tg(fli1:nEGFP)*^{y7} zebrafish were subjected to morpholino oligonucleotide injection of Dll4 or Flt1 or to treatment with inhibitors (3PO, YN1, SU5416). Assessment of sprouting and hyperbranching of ISVs, imaging, and morphometric quantitation was as detailed in the Supplemental Experimental Procedures.

Mouse Models of Ocular Angiogenesis

CNV was induced in C57BL/6 mice by laser burn. Mice were injected intraperitoneally (i.p.) with 38–50 mg/kg PFKFB3 inhibitor 3PO daily with or without treatment with anti-VEGFR2 DC101 (12.5 mg/kg i.p., 3× per week). Eyes were enucleated 2 weeks after the laser treatment and processed for immunohistochemistry and neovascular morphometric analysis as described in the Supplemental Experimental Procedures. Oxygen-induced retinopathy was induced by exposing C57BL/6 pups to 70% oxygen from P7–P12. Pups were then returned to normoxia and injected daily with 70 mg/kg 3PO and euthanized at P17. Retinal flat mounts were analyzed as described in the Supplemental Experimental Procedures. For analysis of neonatal retinal angiogenesis, mice were injected with 50 mg/kg 3PO or vehicle between P2 and P4 and euthanized at P4 or P5; eyes were enucleated and fixed, and retinal flat mounts were prepared for vascular analysis as described in the Supplemental Experimental Procedures.

Mouse Models of Inflammation

Skin inflammation was induced by daily topical application of 5% imiquimod cream on the back of BALB/c mice. Mice received a daily i.p. dose of 50 mg/kg 3PO. After 4 days, skins were resected for analyses as described in the Supplemental Experimental Procedures. Acute colitis was induced with 2.5% dextran sodium sulfate (DSS) in the drinking water for 6 days. Mice received a daily i.p. dose of 50mg/kg 3PO. Histological scoring was as detailed in the Supplemental Experimental Procedures. All experimental animal procedures were approved by the Institutional Animal Care and Research Advisory Committee of the University of Leuven.

Statistics

Data represent mean ± SEM of representative experiments, unless otherwise stated. For all in vitro and in vivo experiments, every experiment was performed at least three times. For analysis of the mouse models of angiogenesis, the investigator assessing the outcome was blinded to the group allocation; for analysis of zebrafish models of angiogenesis, assessment was done by an investigator ignorant of potential outcome. Unless otherwise indicated, statistical significance between groups was calculated by standard t test with F testing to confirm equality of variance (Prism v4.0b). Phenotype severity distributions were analyzed by chi-square test. Statistical significance of DAI and histological scoring data were determined by Mann-Whitney test. $p < 0.05$ was considered statistically significant.

SUPPLEMENTAL INFORMATION

Supplemental Information includes Supplemental Experimental Procedures, six figures, and one movie and can be found with this article online at http://dx.doi.org/10.1016/j.cmet.2013.11.008.

AUTHOR CONTRIBUTIONS

P.C., S.S., K.D.B., A.R.C., and M.G. conceived and designed the experiments. S.S. and A.R.C. performed the inflammation and ocular models of angiogenesis. All in vitro experiments were performed by S.S., K.D.B., A.R.C., and M.G. The manuscript was written by P.C., S.S., and K.D.B.

ACKNOWLEDGMENTS

We acknowledge the work of Leen Notebaert for help with the illustrations. K.D.B., A.R.C., and B.G. are Postdoctoral Fellows of the Research Foundation-Flanders (FWO); M.G. and S.S. received funding as Emmanuel Vanderschueren fellows of the Flemish Association against Cancer (VLK); and S.S. was funded by the Institution of Research and Innovation (IWT). The work of P.C. is supported by a Federal Government Belgium grant (IUAP7/03), long-term structural Methusalem funding by the Flemish Government, a Concerted Research Activities Belgium grant (GOA2006/11), grants from the FWO (G.0532.10, G.0817.11, G.0834.13, 1.5.202.10N, G.0764.10N, and 1.5.142.13N Krediet aan navorsers), the Foundation Leducq Transatlantic Network (ARTEMIS), the Foundation against Cancer, and the ERC Advanced Research Grant (EU-ERC269073). M.D. is supported by FWO grant G.0598.12. M.C. is supported by the Spanish Government and the European Union FEDER funds (SAF2011-25726), Generalitat de Catalunya-AGAUR (2009SGR1308), and the "ICREA Academia prize." P.C. declares being named as inventor on patent applications claiming subject matter related to the results described in this paper. J.C. is coinventor of US patent #8,088,385 (PFKFB3 inhibitors for the treatment of proliferative cancer).

Received: June 14, 2013
Revised: October 21, 2013
Accepted: November 6, 2013
Published: December 12, 2013

REFERENCES

Cavallaro, G., Filippi, L., Bagnoli, P., La Marca, G., Cristofori, G., Raffaeli, G., Padrini, L., Araimo, G., Fumagalli, M., Groppo, M., et al. (2013). The pathophysiology of retinopathy of prematurity: an update of previous and recent knowledge. Acta Ophthalmol. (Copenh.). Published online April 26, 2013. http://dx.doi.org/10.1111/aos.12049.

Chesney, J., Mitchell, R., Benigni, F., Bacher, M., Spiegel, L., Al-Abed, Y., Han, J.H., Metz, C., and Bucala, R. (1999). An inducible gene product for 6-phosphofructo-2-kinase with an AU-rich instability element: role in tumor cell glycolysis and the Warburg effect. Proc. Natl. Acad. Sci. USA *96*, 3047–3052.

Clem, B., Telang, S., Clem, A., Yalcin, A., Meier, J., Simmons, A., Rasku, M.A., Arumugam, S., Dean, W.L., Eaton, J., et al. (2008). Small-molecule inhibition of 6-phosphofructo-2-kinase activity suppresses glycolytic flux and tumor growth. Mol. Cancer Ther. *7*, 110–120.

Clem, B.F., O'Neal, J., Tapolsky, G., Clem, A.L., Imbert-Fernandez, Y., Kerr, D.A., 2nd, Klarer, A.C., Redman, R., Miller, D.M., Trent, J.O., et al. (2013). Targeting 6-phosphofructo-2-kinase (PFKFB3) as a therapeutic strategy against cancer. Mol. Cancer Ther. *12*, 1461–1470.

Climent, F., Roset, F., Repiso, A., and Pérez de la Ossa, P. (2009). Red cell glycolytic enzyme disorders caused by mutations: an update. Cardiovasc. Hematol. Disord. Drug Targets *9*, 95–106.

Cummins, E.P., Seeballuck, F., Keely, S.J., Mangan, N.E., Callanan, J.J., Fallon, P.G., and Taylor, C.T. (2008). The hydroxylase inhibitor dimethyloxalylglycine is protective in a murine model of colitis. Gastroenterology *134*, 156–165.

Darlow, B.A., Ells, A.L., Gilbert, C.E., Gole, G.A., and Quinn, G.E. (2013). Are we there yet? Bevacizumab therapy for retinopathy of prematurity. Arch. Dis. Child. Fetal Neonatal Ed. *98*, F170–F174.

De Bock, K., Georgiadou, M., and Carmeliet, P. (2013a). Role of endothelial cell metabolism in vessel sprouting. Cell Metab. *18*, 634–647.

De Bock, K., Georgiadou, M., Schoors, S., Kuchnio, A., Wong, B.W., Cantelmo, A.R., Quaegebeur, A., Ghesquière, B., Cauwenberghs, S., Eelen, G., et al. (2013b). Role of PFKFB3-driven glycolysis in vessel sprouting. Cell *154*, 651–663.

Ebos, J.M., and Kerbel, R.S. (2011). Antiangiogenic therapy: impact on invasion, disease progression, and metastasis. Nat Rev Clin Oncol *8*, 210–221.

François, J., Eraso, P., and Gancedo, C. (1987). Changes in the concentration of cAMP, fructose 2,6-bisphosphate and related metabolites and enzymes in Saccharomyces cerevisiae during growth on glucose. Eur. J. Biochem. *164*, 369–373.

Geudens, I., and Gerhardt, H. (2011). Coordinating cell behaviour during blood vessel formation. Development *138*, 4569–4583.

Granchi, C., and Minutolo, F. (2012). Anticancer agents that counteract tumor glycolysis. ChemMedChem *7*, 1318–1350.

Harjes, U., Bensaad, K., and Harris, A.L. (2012). Endothelial cell metabolism and implications for cancer therapy. Br. J. Cancer *107*, 1207–1212.

Hellström, M., Phng, L.K., Hofmann, J.J., Wallgard, E., Coultas, L., Lindblom, P., Alva, J., Nilsson, A.K., Karlsson, L., Gaiano, N., et al. (2007). Dll4 signalling through Notch1 regulates formation of tip cells during angiogenesis. Nature *445*, 776–780.

Herrero-Mendez, A., Almeida, A., Fernández, E., Maestre, C., Moncada, S., and Bolaños, J.P. (2009). The bioenergetic and antioxidant status of neurons is controlled by continuous degradation of a key glycolytic enzyme by APC/C-Cdh1. Nat. Cell Biol. *11*, 747–752.

Hindryckx, P., Waeytens, A., Laukens, D., Peeters, H., Van Huysse, J., Ferdinande, L., Carmeliet, P., and De Vos, M. (2010). Absence of placental growth factor blocks dextran sodium sulfate-induced colonic mucosal angiogenesis, increases mucosal hypoxia and aggravates acute colonic injury. Lab. Invest. *90*, 566–576.

Krueger, J., Liu, D., Scholz, K., Zimmer, A., Shi, Y., Klein, C., Siekmann, A., Schulte-Merker, S., Cudmore, M., Ahmed, A., and le Noble, F. (2011). Flt1 acts as a negative regulator of tip cell formation and branching morphogenesis in the zebrafish embryo. Development *138*, 2111–2120.

Lalwani, G.A., Rosenfeld, P.J., Fung, A.E., Dubovy, S.R., Michels, S., Feuer, W., Davis, J.L., Flynn, H.W., Jr., and Esquiabro, M. (2009). A variable-dosing regimen with intravitreal ranibizumab for neovascular age-related macular degeneration: year 2 of the PrONTO Study. Am. J. Ophthalmol. *148*, 43–58, e1.

Leopold, J.A., Walker, J., Scribner, A.W., Voetsch, B., Zhang, Y.Y., Loscalzo, A.J., Stanton, R.C., and Loscalzo, J. (2003). Glucose-6-phosphate dehydrogenase modulates vascular endothelial growth factor-mediated angiogenesis. J. Biol. Chem. *278*, 32100–32106.

Locasale, J.W., and Cantley, L.C. (2010). Altered metabolism in cancer. BMC Biol. *8*, 88.

Lunt, S.Y., and Vander Heiden, M.G. (2011). Aerobic glycolysis: meeting the metabolic requirements of cell proliferation. Annu. Rev. Cell Dev. Biol. *27*, 441–464.

Miller, J.W., Le Couter, J., Strauss, E.C., and Ferrara, N. (2013). Vascular endothelial growth factor a in intraocular vascular disease. Ophthalmology *120*, 106–114.

Niranjan, H.S., Benakappa, N., Reddy, K.B., Nanda, S., and Kamath, M.V. (2012). Retinopathy of prematurity promising newer modalities of treatment. Indian Pediatr. *49*, 139–143.

Potente, M., Gerhardt, H., and Carmeliet, P. (2011). Basic and therapeutic aspects of angiogenesis. Cell *146*, 873–887.

Raez, L.E., Papadopoulos, K., Ricart, A.D., Chiorean, E.G., Dipaola, R.S., Stein, M.N., Rocha Lima, C.M., Schlesselman, J.J., Tolba, K., Langmuir, V.K., et al. (2013). A phase I dose-escalation trial of 2-deoxy-D-glucose alone or combined with docetaxel in patients with advanced solid tumors. Cancer Chemother. Pharmacol. *71*, 523–530.

Rofagha, S., Bhisitkul, R.B., Boyer, D.S., Sadda, S.R., and Zhang, K.; SEVEN-UP Study Group (2013). Seven-Year Outcomes in Ranibizumab-Treated Patients in ANCHOR, MARINA, and HORIZON: A Multicenter Cohort Study (SEVEN-UP). Ophthalmology *120*, 2292–2299.

Sacharidou, A., Stratman, A.N., and Davis, G.E. (2012). Molecular mechanisms controlling vascular lumen formation in three-dimensional extracellular matrices. Cells Tissues Organs (Print) *195*, 122–143.

Scott, A., and Fruttiger, M. (2010). Oxygen-induced retinopathy: a model for vascular pathology in the retina. Eye (Lond.) *24*, 416–421.

Seo, M., Kim, J.D., Neau, D., Sehgal, I., and Lee, Y.H. (2011). Structure-based development of small molecule PFKFB3 inhibitors: a framework for potential cancer therapeutic agents targeting the Warburg effect. PLoS ONE *6*, e24179.

Singh, M., and Ferrara, N. (2012). Modeling and predicting clinical efficacy for drugs targeting the tumor milieu. Nat. Biotechnol. *30*, 648–657.

Stewart, M.W. (2012). The expanding role of vascular endothelial growth factor inhibitors in ophthalmology. Mayo Clin. Proc. *87*, 77–88.

Telang, S., Clem, B.F., Klarer, A.C., Clem, A.L., Trent, J.O., Bucala, R., and Chesney, J. (2012). Small molecule inhibition of 6-phosphofructo-2-kinase suppresses t cell activation. J. Transl. Med. *10*, 95.

Van de Veire, S., Stalmans, I., Heindryckx, F., Oura, H., Tijeras-Raballand, A., Schmidt, T., Loges, S., Albrecht, I., Jonckx, B., Vinckier, S., et al. (2010). Further pharmacological and genetic evidence for the efficacy of PlGF inhibition in cancer and eye disease. Cell *141*, 178–190.

Van Schaftingen, E., Lederer, B., Bartrons, R., and Hers, H.G. (1982). A kinetic study of pyrophosphate: fructose-6-phosphate phosphotransferase from potato tubers. Application to a microassay of fructose 2,6-bisphosphate. Eur. J. Biochem. *129*, 191–195.

Wynn, T.A., Chawla, A., and Pollard, J.W. (2013). Macrophage biology in development, homeostasis and disease. Nature *496*, 445–455.

Yalcin, A., Telang, S., Clem, B., and Chesney, J. (2009). Regulation of glucose metabolism by 6-phosphofructo-2-kinase/fructose-2,6-bisphosphatases in cancer. Exp. Mol. Pathol. *86*, 174–179.